2014 SCEC Final Report – Project 14113
Estimating Fault Zone Properties From Seismic Fault Zone Trapped Noise

G. Hillers (UJF Grenoble, France) and Y. Ben-Zion (USC Los Angeles, USA)

Abstract
Systematic velocity contrasts across and within fault zones can produce head and trapped waves that provide direct information on structural units that are important for many aspects of earthquake and fault mechanics. We discovered a new type of seismological signature, fault zone trapped noise (Hillers et al. 2014), that extends the range of previously known ballistic fault zone waves. Analyzing data from the Calico field experiment we studied the interaction of the ambient seismic wavefield with a fault zone environment; we showed that the high-frequency wavefield in the fault differs from the field in the adjacent crust. Noise within the fault is characterized by significantly increased isotropy, which indicates that randomization of propagation directions is more efficient, and energy can be considered as trapped. We showed that conditions controlling the emergence of seismic fault zone trapped noise have less limitations compared to trapped ballistic waves.

We proposed to investigate the potential of the correlation field associated with trapped noise to provide a high resolution tool for imaging the internal structure (dimensions, seismic velocity, attenuation, continuity) of fault damage zones, in analogy to properties of fault zone trapped waves (e.g., Li et al., 1990, 1994; Ben-Zion et al., 2003; Lewis et al., 2005). We construct noise correlation functions from the scattered seismic wavefield recorded by a spatially dense array with >1100 vertical-component nodes separated by 10 – 30 m centered on the Clark segment of the San Jacinto Fault Zone southeast of Anza (BenZion et al., 2015). Based on estimates of the similarity of causal and acausal waveforms we assess the noise correlation symmetry, which is an indicator of noise wavefield isotropy. Spatial distributions of similarity and hence isotropy markers can be indicative of trapping and waveguiding structures.

SCEC priorities
Our preliminary results of an innovative imaging tool based on correlation functions in a fault zone environment are a means of addressing SCEC Research Priorities 1a, 4b, and 6a. The approach contributes directly to the SCEC4 long-term research goal to benefit from the densification of seismic instrumentation, and to FARM's focus area for the determination of fault properties and the characterization of damage zone variability along strike.

Intellectual Merit
Fault zone trapped noise has only recently been discovered and described. Additional analyses targeting manifestations of this signature help to assess the generality of its occurrence, and its applicability for fault zone imaging.

Broader Impact
The study constitutes a novel approach to analyze noise correlation functions constructed from data collected by a very dense array, a configuration that many regard as a blueprint for future seismological investigations. Our symmetry analysis targets systematic wavefield variations occurring in fault zone environments. Results can yield images of mechanically important waveguide units associated with low velocity fault damage zones.

Technical Report

The ambient seismic noise field has been used extensively in the last decade to image numerous structures across a wide range of spatial scales ranging from the lithosphere and upper mantel at local, regional, and continental distances (Vandemeulebrouck et al., 2009; Shapiro et al., 2005; Verbeke et al., 2012) to the core of the Earth (Lin et al., 2013). Noise based imaging requires that the ambient wave field is produced by sufficiently isotropic noise sources, since strong wave field directionality biases Green's function estimates from noise correlations (Weaver et al., 2009). Scattering plays a significant role in the randomization of propagation directions at long lapse times, and greatly contributes to the applicability of noise based imaging techniques. Seismic heterogeneities control the efficiency of this mode mixing process, and range from relatively homogeneous cratonic areas (Poli et al., 2013) to highly scattering volcanic edifices (Wegler, 2003) and fault zone (FZ) environments (Revenaugh, 2000; Hong and Menke, 2006; Hillers et al., 2013a).

Extending these traditional approaches, we discovered a new type of seismological signature, fault zone trapped noise (Hillers et al., 2014). This refers to the high-frequency wavefield within an low velocity waveguiding zone that is characterized by significantly increased isotropy compared to the ambient field outside the FZ. We extend the original observation made with data from the Calico fault zone experiment to investigate the potential of noise correlation functions constructed from the trapped FZ noise wavefield to provide a high resolution imaging tool. A key manifestation of the more isotropic trapped noise field is the increased symmetry of correlation functions constructed between stations located within the trapping cavity-like structure compared to stations located outside the FZ. We analyzed symmetry properties of noise correlation functions using vertical component data from a spatially-dense Nodal array that straddles the damage zone of the Clark branch of the San Jacinto fault southeast of Anza (Ben-Zion et al., 2015). In this initial study we focused on two lines in fault-normal directions (Fig. 1). A systematic assessment of directional (azimuthal) wavefield changes requires the computationally challenging constructions of all-to-all correlation pairs, and will thus be subject of future work.

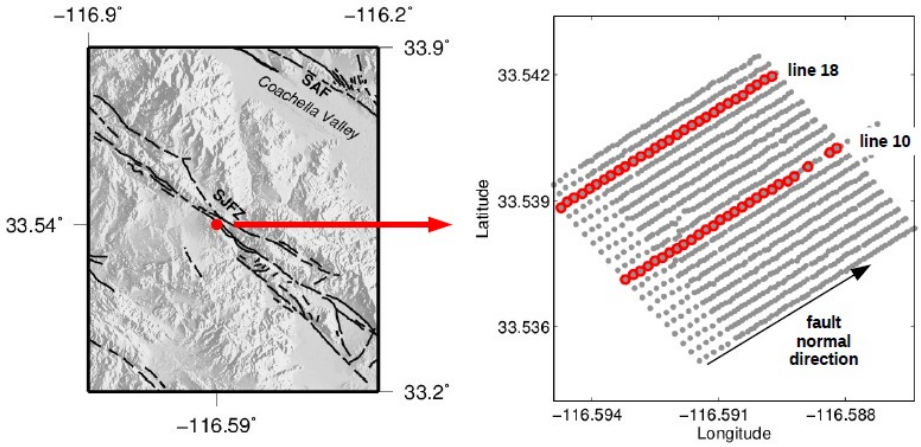

Figure 1 (Left) Map of the San Jacinto fault zone area. The red dot indicates the location of the Nodal-array. (Right) Configuration of the Nodal-array. We used data from lines 10 and 18.

Analysis

Construction of noise correlation functions

We apply data preprocessing consisting of a high-pass filter, glitch removal, whitening (0.5 – 25 Hz) of 30 minute segments, and threshold clipping at three times the standard deviation of the amplitude distribution in each segment. Data are cross-correlated and stacked over 20 days. Broadband cross-correlation functions are bandpass filtered to study the frequency dependent response (Fig. 2). The optimization of the signal-to-noise ratio using different preprocessing parameters is the subject of ongoing work.

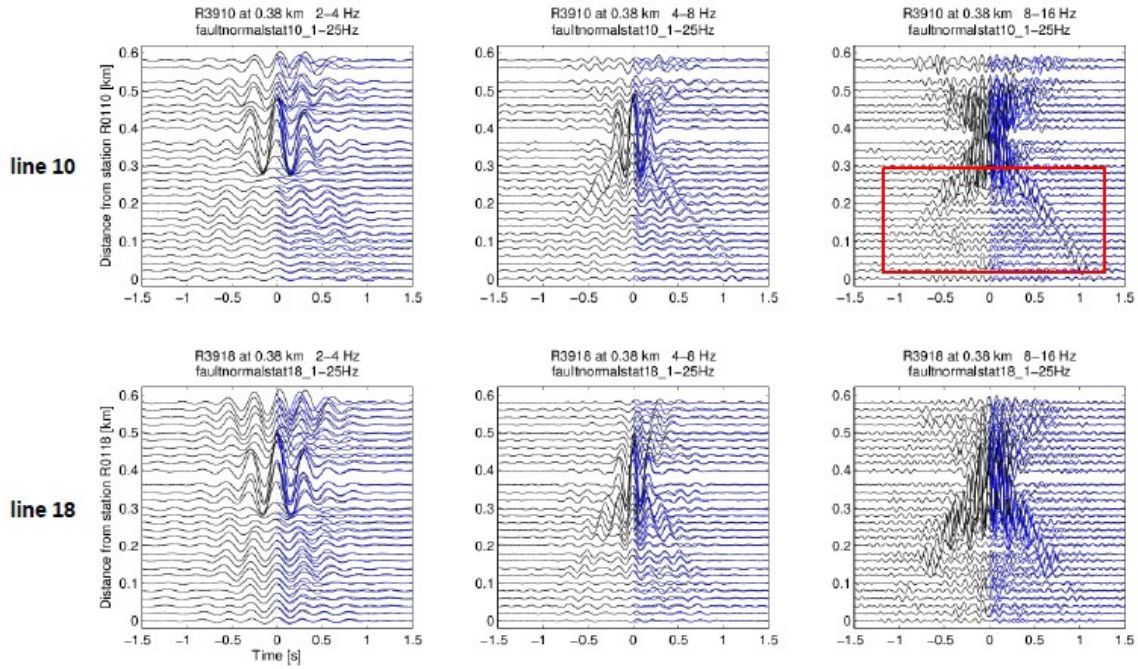

Figure 2 Example noise correlation wavefields for different frequency bands (left to right) obtained from the two lines (top and bottom). The reference station is located just below 0.4 km. Blue waveforms are the flipped acausal part of the correlation function. The red box in the upper right highlights waveform dissimilarities at positive and negative lag times that are indicative of propagation regimes and thus structural units.

Assessment of waveform similarity

Our goal is to quantify the noise correlation waveform similarity at negative and positive lag times in a fixed window around the direct surface wave arrival as a function of the fault-perpendicular location (Fig. 2). Again, this similarity can be an indicator of the propagation regime, where high causal-acausal similarity constitutes an isotropy marker. There are multiple ways to quantify waveform symmetry or similarity. We tested a time and a frequency domain approach (Fig. 3):

[1] We multiply the two waveforms and sum (the result depends on the relative amplitudes).

[2] We estimate the spectral similarity using a cross power spectral density (the result depends on the coherent energy in the spectral domain).

We compute estimates for each correlation pair along the line. To reduce the possibility of distance dependent bias, we keep only pairs within a range that is defined as the minimum of all maximum correlation distances of all pairs. The measurements are scaled by the median of a smoothed maximum amplitude estimate.

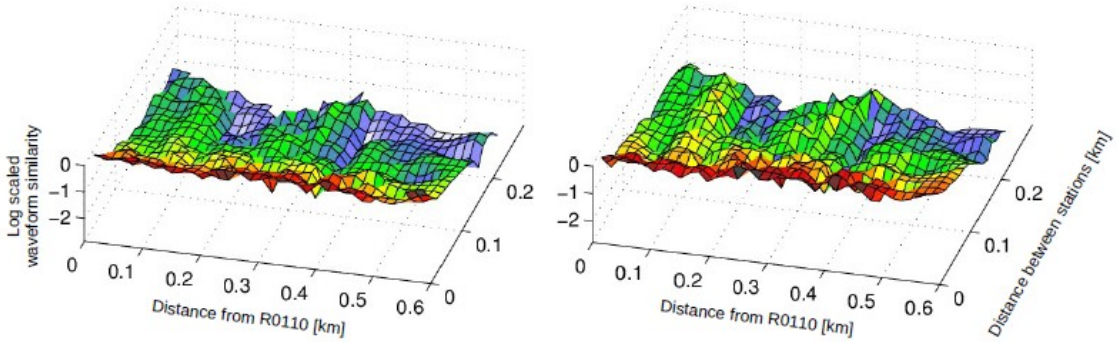

Figure 3 Results obtained with similarity estimates 1 (left) and 2 (right). The x-axis corresponds to the fault-normal position of the reference station. The y-axis is the absolute distance between a correlation station pair. The z-axis is the magnitude of the estimator.

Results

Similarity measurements based on the two estimates are very similar and mutually support each other (Fig 3). We find (Fig. 4) higher (far field) waveform similarity estimates at fault-normal distances greater than 0.3 km at low frequencies (2 – 4 Hz). This can be an indicator of different wave propagation regimes associated with a material contrast across the fault. At intermediate frequencies (6 – 12 Hz) the 3D plots do not indicate a specific trend. However, the (near field) maximum amplitude distribution (inset) implies higher waveform similarities around 0 and 0.3 km. The high frequency (10 – 20 Hz) correlation wavefield shows a distinct far field pattern. It is characterized by high similarities around 0.1, 0.3, and 0.5 km, and by low estimates in between, at 0.2 and 0.4 km.

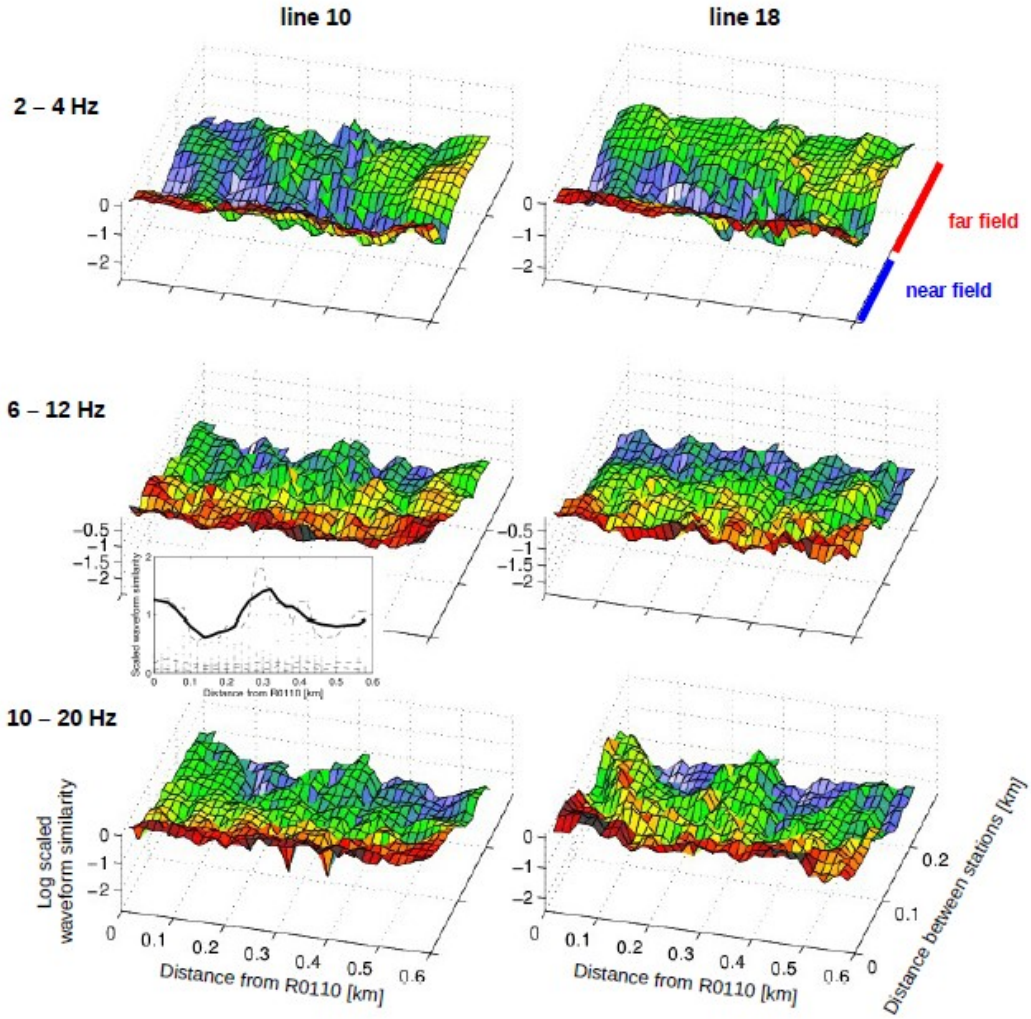

Figure 4 (Exemplary figure.) Frequency dependence (top to bottom) of the cross-correlation waveform similarity estimator based on coherent energy in the spectral domain. The x-axis corresponds to the fault-normal position of the reference station. The y-axis is the absolute distance between a correlation station pair. The z-axis is the magnitude of the estimator. At high frequencies (bottom row) low far field values indicate a propagation barrier around fault normal distance 0.2 and 0.4 km.

These findings show a frequency dependent effect of the medium properties on correlation waveform symmetry or similarity. Whereas the low-frequency response is indicative of a material contrast, the high-frequency patterns indicate 'similarity barriers' (the blue troughs) that are likely associated with structural units.

In the original observations from the Calico fault zone environment we found a critical frequency that defines a threshold above which the in-fault scattered wavefield has increased isotropy and coherency compared to the ambient noise. Spectral properties of trapped waves exhibit the same sensitivity to the FZ structure, which confirms a consistent critical frequency for interaction that applies to ballistic and scattered wavefields alike. Clearly, the size of the trapping waveguide/cavity-like structure in relation to the wavelength governs this critical frequency. The San Jacinto Nodal array results are compatible with this notion and indicate a similar frequency dependent sensitivity.

Focusing on the high-frequency pattern (10 – 20 Hz), the 'similarity barriers' can be compared to results discussed in Ben-Zion et al. (2015). Both a high-frequency fault-normal Rayleigh wave group velocity profile and the spatial energy distribution indicate two zones of reduced velocities that exhibit above-average energy. The fault-normal position of these low velocity zones coincides with the position of our barriers. This is in contrast to the hypothesis underlying our analysis, according to which the low-velocity, high-amplitude zones trap energy and thus lead to more similar correlation waveforms. The opposite is observed. The consistency between our far-field similarity distribution (a fault-normal profile at e.g. 0.2 km station-distance) and the results by Ben-Zion et al. (2015) nevertheless suggest that our estimates are governed by fault-normal variations of medium properties.

Conclusions

Our preliminary noise correlation similarity estimates from data of the San Jacinto Nodal array provide new observables that extend the range of classic imaging approaches. This can lead to stronger joint constraints in this complex faulting environment, and can support estimates of internal FZ properties by comparing results from our noise analysis to traditional ballistic-based approaches. A refinement of our approach and extension to the complete dataset is targeted for the next visit of G. Hillers to USC.

Products supported by this SCEC funding

We presented these results at the 2014 SCEC meeting:

G. Hillers, Y. Ben-Zion, M. Campillo, P. Roux, and F. L. Vernon, “Seismic Trapped Noise in the San Jacinto Fault Zone Southeast of Anza”, Annual SCEC Meeting, Palm Springs, Poster 184, 2014

References

Ben-Zion, Y., Z. Peng, D. Okaya, L. Seeber, J. G. Armbruster, N. Ozer, A. J. Michael, S. Baris, and M. Aktar (2003), A shallow fault zone structure illuminated by trapped waves in the Karadere-Duzce branch of the North Anatolian Fault, western Turkey, Geophys. J. Int. , 152 , 699-717.

Ben-Zion, Y., et al. (2015), Basic data features and results from a spatially-dense seismic array on the San Jacinto fault zone, Geophys. J. Int., revised.

Hillers, G., Y. Ben-Zion, M. Landes, and M. Campillo (2013), Interaction of microseisms with crustal heterogeneity: A case study from the San Jacinto fault zone area, Geochem. Geophys. Geosyst. , 14 (7), doi:10.1002/ggge.20140.

Hillers, G., M. Campillo, Y. Ben-Zion, and P. Roux (2014), Seismic fault zone trapped noise, J. Geophy. Res. , 119 (7), 5786-5799, doi:10.1002/2014JB011217.

Hong, T.-K., and W. Menke (2006), Tomographic investigation of the wear along the San Jacinto fault, southern California, Phys. Earth Planet. Inter.,155 , 236-248.

Lewis, M. A., Z. Peng, Y. Ben-Zion, and F. L. Vernon (2005), Shallow seismic trapping structure in the San Jacinto fault zone near Anza, California, Geophys. J. Int. , 162 , 867-881, doi:10.1111/j.1365-246X.2005.02684.x.

Li, Y.-G., P. Leary, K. Aki, and P. Malin (1990), Seismic Trapped Modes in the Oroville and San Andreas Fault Zones, Science , 249 (4970), 763-766, doi:10.1126/science.249.4970.763.

Li, Y.-G., K. Aki, D. Adams, A. Hasemi, and W. H. K. Lee (1994), Seismic guided waves trapped in the fault zone of the Landers, California, earthquake of 1992, J. Geophy. Res. , 99 (B6), 11,705-11,722.

Poli, P., H. A. Pedersen, M. Campillo, and the POLENET/LAPNET Working Group (2013), Noise directivity and group velocity tomography in a region with small velocity contrasts: the northern Baltic shield, Geophys. J. Int., 192 , 413-424, doi:10.1093/gji/ggs034.

Revenaugh, J. (2000), The relation of crustal scattering to seismicity in southern California, J. Geophy. Res. , 105 (B11), 25,403-25,422.

Shapiro, N. M., M. Campillo, L. Stehly, and M. H. Ritzwoller (2005), High-Resolution Surface-Wave Tomography from Ambient Seismic Noise, Science, 307, 1615-1618, doi:10.1126/science.1108339.

Vandemeulebrouck, J., R. Roux, P. Gouedard, A. Legaz, A. Revil, A. W. Hurst, A. Boleve, and A. Jardani (2009), Application of acoustic noise and self-potential localization techniques to a buried hydrothermal vent (Waimangu Old Geyser site, New Zealand), Geophys. J. Int., 180, 883-890, doi:10.1111/j.1365-246X.2009.04454.x.

Verbeke, J., L. Boschi, L. Stehly, E. Kissling, and A. Michelini (2012), High-resolution Rayleigh-wave velocity maps of central Europe from a dense ambient-noise data set, Geophys. J. Int., 188, 1173-1187, doi:10.1111/j.1365-246X.2011.05308.x.

Weaver, R. L., B. Froment, and M. Campillo (2009), On the correlation of non-isotropically distributed ballistic scalar di
use waves, J. Acoust. Soc. Am., 126 (4), 1817-1826, doi:10.1121/1.3203359.

Wegler, U. (2003), Analysis of multiple scattering at Vesuvius volcano, Italy, using data of the TomoVes active seismic experiment, J. Volcanol. Geotherm. Res., 128, 45-63, doi:10.1016/S0377-0273(03)00246-4.